Communication

A Compact-Size and High-Efficiency Cage Antenna for 2.4-GHz WLAN Access Points

Zhenyu Liu, Yongjian Zhang, Yijing He, and Yue Li

***Abstract*— In this communication, a compact-size and high-efficiency air cavity antenna with a cage-like structure is proposed for 2.4 GHz wireless local area networks (WLAN). The air cavity antenna is constructed with four sides of hybrid metallized vias, including sparsely arranged blind vias and tightly arranged shorting vias. First, the antenna size is significantly reduced by utilizing the shorting vias, which makes the antenna operate at the high-order $TM_{1/2,1/2}$ mode. Then, by loading the capacitive blind vias at the radiating apertures, the antenna size is further miniaturized. Notably, high radiation efficiency is obtained attributed to the lower dielectric loss of the air-medium structure. Finally, a prototype of the proposed cage antenna has been fabricated and tested with good agreement between simulated and measured results. In such a compact size of $0.128\lambda_0 \times 0.128\lambda_0 \times 0.10\lambda_0$ (λ_0 is the free-space wavelength at the center frequency), the measured total efficiency over 90% is achieved in the WLAN band by the cage structure. Compared with the existing 2.4 GHz antennas, the proposed one is with the ascendency of compact size and high radiating efficiency for WLAN applications.**

***Index Terms*— Antenna miniaturization, antenna radiation efficiency, cavity antennas, hybrid metallic vias, microstrip antennas.**

I. Introduction

With the development of wireless techniques, the integration level of the modern communication systems speeds up, and consequently, miniaturized antennas are increasingly popular for space-limited devices [1], [2], [3], [4], [5], [6], [7], [8], [9], [10], [11]. Furthermore, for the application of wireless local area networks (WLAN), antennas with high radiation efficiency are also essentially demanded to provide high-speed, low-latency, and reliable communication services.

To this day, a lot of feasible methods have been propounded to realize antenna miniaturization. The first approach is applying the high-permittivity substrate to the antenna design [12], [13]. Another effective method is using meandered or fractal structures. In this way, by extending the current path and optimizing the antenna shape, the operating frequency can be downshifted, and thus, the antenna is miniaturized [14], [15], [16]. Besides, there is a slot-loading technique sharing the similar meandering principle. The slots loaded on the surface of planar antennas allow the electric current to travel along a longer path, leading to less realization area [17], [18], [19]. Metamaterial-loading structures have also been investigated as antenna miniaturization elements. For instance, the split ring resonators (SRRs) are widely utilized as loading structures to reduce the resonance frequency [20], [21], [22], [23], [24]. In addition, there are other methods of antenna miniaturization, such as the frequency reconfigurable antenna loaded with lumped *LC* elements or pin diodes [25], [26], [27], [28] and the nonfoster antennas with active transistors [29], [30], [31]. However, all the methods mentioned above are with a common problem of low radiation efficiency. Chu [32] and Harington [33] indicated that the antenna's bandwidth and radiation efficiency are restricted by its size. With the miniaturization of the antenna size, the bandwidth or radiation efficiency is usually deteriorated [34], [35]. To increase the radiation efficiency, a typical method is adopting microelectromechanical systems (MEMS) process for low-loss air cavity, and the antenna's efficiency is increased significantly, e.g., up to 90% [36], [37], [38].

In this communication, we propound an uncomplicated but practicable approach to realize an antenna with both compact size and high efficiency. Based on the design method, the proposed antenna comprises two various types of metallized vias, demonstrating the effect on antenna miniaturization. Specifically, two arrays of shorting vias provide short-circuit boundaries, and thus, the antenna can operate at a high-order mode with obviously reduced size. What is more, attributed to the other two sets of capacitive blind vias loaded on the radiation apertures, the size of the antenna is further miniaturized without changing the operating frequency. Last but not least, by exploiting the air cavity with low dielectric loss, the goal for high efficiency is fulfilled within such a compact antenna size. Compared with [39], we apply two different kinds of metallic vias instead of the single blind-via fence. As a consequence, the propounded antenna is with smaller size and higher radiation efficiency than the method proposed in [39]. In the following, numerical and experimental results are presented for validation.

II. Antenna Design and Operating Principles

The geometry of the proposed antenna is shown in Fig. 1. The proposed cage antenna is composed of a top square radiating patch, two rows of sparsely arranged blind vias, two rows of tightly arranged shorting vias, and dielectric substrate with metal printed on its back. The metallized patch is manufactured on a 2 mm F4BM dielectric substrate whose permittivity is 2.65 and loss tangent is 0.002. The sets of blind vias are loaded on the two sides of radiating apertures, with diameter (D_1), period (p_1), and gap (g) to the metallic ground. The sets of shorting vias with diameter (D_2) and period (p_2) are placed along the other two sides. These blind vias share the same size as that of the holes drilled on the upper substrate. The thickness (g) of the dielectric with ground printed on the back is 2 mm, and it serves as a structural support for the cage structure. As shown in Fig. 1(b), the metallic patch and substrate with ground plane are both square and with the side length of W and W_g, respectively. Fig. 1(c) shows the front and back cross-sectional views of the propounded antenna. Clearly, the upper patch is physically connected to both blind vias

Manuscript received 11 July 2022; revised 16 September 2022; accepted 17 September 2022. Date of publication 30 September 2022; date of current version 22 December 2022. This work was supported in part by the National Natural Science Foundation of China under Grant 62022045, in part by the National Key Research and Development Program of China under Grant 2021YFA0716600, and in part by the Shenzhen Science and Technology Program under Grant JSGG20210802153800002. *(Corresponding author: Yue Li.)*

Zhenyu Liu, Yongjian Zhang, and Yue Li are with the Department of Electronic Engineering, Beijing National Research Center for Information Science and Technology, Tsinghua University, Beijing 100084, China (e-mail: lyee@tsinghua.edu.cn).

Yijing He is with the Electronic Engineering Department, Beijing Institute of Technology, Beijing 100081, China.

Color versions of one or more figures in this communication are available at https://doi.org/10.1109/TAP.2022.3209327.

Digital Object Identifier 10.1109/TAP.2022.3209327

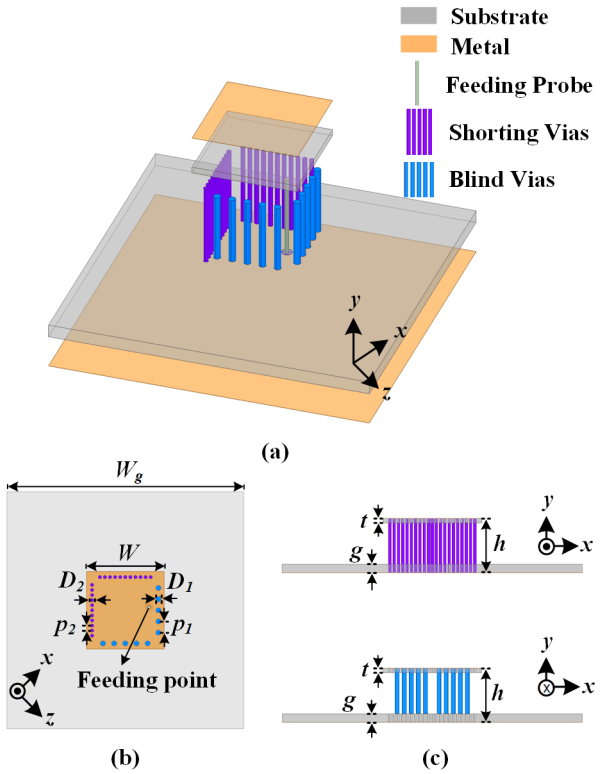

Fig. 1. Configuration of the proposed antenna: (a) perspective view, (b) top view, and (c) cross-sectional view.

TABLE I
DETAILED DIMENSIONS

Parameter	Value (mm)	Parameter	Value (mm)	Parameter	Value (mm)
W_g	49.0	D_2	0.7	g	2.0
W	16.1	p_1	2.3	t	1.0
D_1	1.1	p_2	1.1	h	12.5

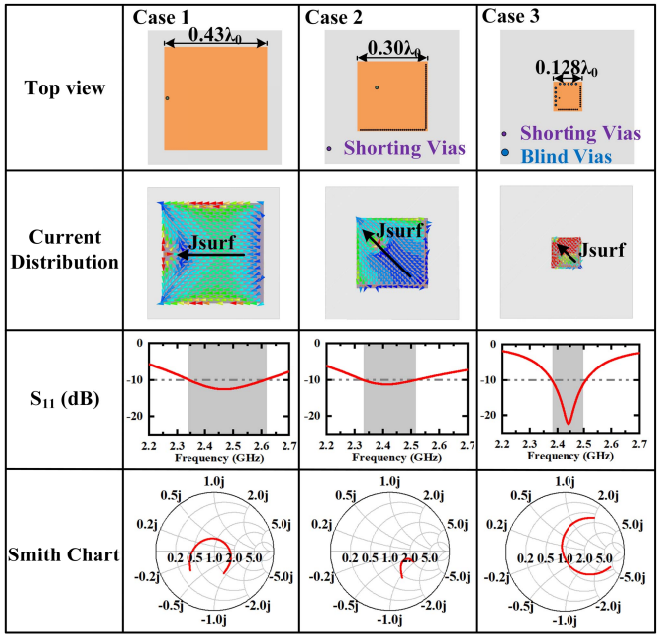

Fig. 2. Comparison of top views of antennas, vector surface current distributions at 2.44 GHz, S_{11}, and Smith chart among the three cases.

and shorting vias. In addition, the shorting vias are connected to the metallic ground, while the blind vias are with the gap to the metallic ground. In order to simplify things, the bottom dielectric substrate with ground printed on its back utilizes the same F4BM material as the dielectric substrate on the top. A 50 Ω semigrid cable is used to feed the propounded antenna, with the inner and outer conductors soldered to the top patch and bottom metallic ground, respectively. The detailed values of geometrical parameters of the propounded antenna are listed in Table I. Here, the commercial software Ansoft High Frequency Structure Simulator (HFSS) is used for optimization.

To exhibit the procedure and degree of miniaturization of the propounded method, Fig. 2 shows the top views, vector surface current distributions, S_{11}, and Smith chart of various cases: 1) the ordinary patch antenna operates at the TM_{10} mode; 2) the patch antenna operates at the $TM_{1/2,1/2}$ mode; and 3) the proposed antenna operates at the $TM_{1/2,1/2}$ mode. For a fair comparison, all the antennas apply air substrate with the equal thickness of 12.5 mm and resonate at the exact same central frequency (2.44 GHz). From Fig. 2, it can be observed that compared with the antenna in Case 2, the size of the antenna manages to reduce 51.3% from $0.43\lambda_0 \times 0.43\lambda_0$ to $0.30\lambda_0 \times 0.30\lambda_0$, where λ_0 is the free-space wavelength at 2.44 GHz. Furthermore, compared with the regular patch antenna presented in Case 1, the size of the proposed antenna is reduced with a ratio up to 91.1% from $0.43\lambda_0 \times 0.43\lambda_0$ to $0.128\lambda_0 \times 0.128\lambda_0$. In Cases 1 and 2, it is hard to match the impedance of the antenna due to the high inductive impedance brought by the thick profile. Therefore, we add the 0.9 pF shunt capacitor and 4 nH series inductor at the port in Case 1. Similarly, the 0.5 pF shunt capacitor and 3.6 nH series inductor are added at the port in Case 2. In contrast, with the loading capacitive blind vias that compensate for the strong inductive impedance, the proposed antenna in Case 3 is with a good impedence matching without the help of the matching elements. For the regular patch antenna, the current shows symmetric distribution with respect to geometric center of the proposed antenna. By contrast, we can see that the current mainly concentrates under the capacitive blind vias for the proposed antenna. In addition, it is worth mentioning that the current distribution is quite weak compared with that in the patch in Case 3. Therefore, slightly varying the size of ground plane only has a minor effect on the maximum gain and minimum gain of the radiation pattern of the proposed antenna.

The design criterion for the propounded antenna is summarized. For engineering requirements, we want to design a miniaturized and high-efficiency antenna, which operates at f_c (f_c is equal to 2.44 GHz in this design) with two kinds of metallized vias. By exploring the law of the three cases, we find that applying the two kinds of the metallized vias causes the operating frequency of the antenna to downshift to lower frequency and reduces the bandwidth. First, we estimate the frequency of the TM_{10} mode patch antenna as f_1 (f_1 is around 8 GHz in this design) by properly scaling the antenna and choose the initial size of the patch antenna as $0.128\lambda_c \times 0.128\lambda_c \times 0.10\lambda_c$, where λ_c represents the wavelength in free space at f_c. Second, we add two rows of shorting vias to make the antenna operate at $TM_{1/2,1/2}$ mode, and a proper number of shorting vias are selected with subwavelength diameter and period. The operating frequency is downshifted from f_1 to f_2 at this time, while f_2 is still greater than f_c (f_2 is around 6 GHz in this design). Third, we load the capacitive blind vias to the other two sides of the antenna and adjust the essential geometrical parameter value of

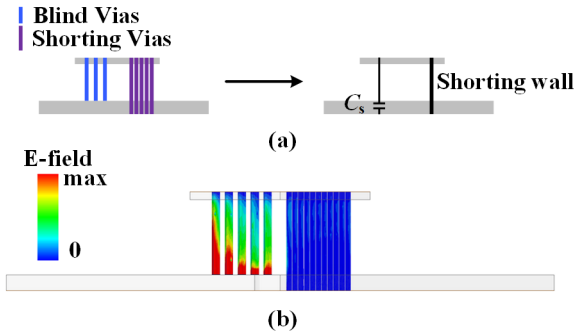

Fig. 3. (a) Equivalent effect of the hybrid metallic vias. (b) E-field magnitude distribution on the hybrid metallic vias at 2.44 GHz.

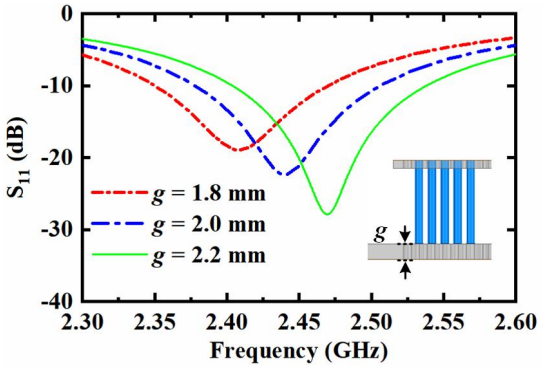

Fig. 4. Simulated S_{11} of the proposed antenna when g is 1.8, 2.0, and 2.2 mm.

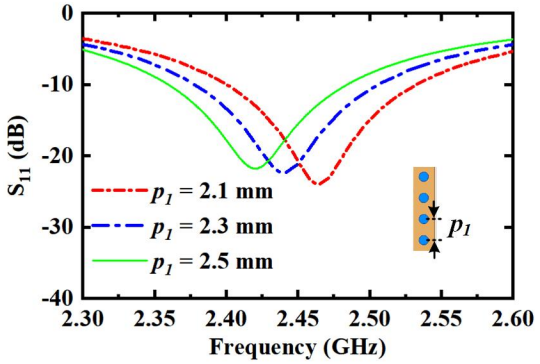

Fig. 5. Simulated S_{11} of the proposed antenna when p_1 is 2.1, 2.3, and 2.5 mm.

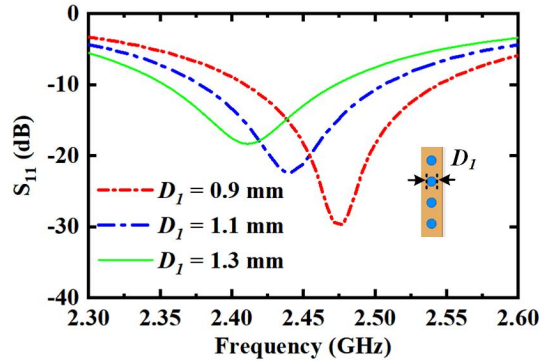

Fig. 6. Simulated S_{11} of the proposed antenna when D_1 is 0.9, 1.1, and 1.3 mm.

the metallic blind vias, e.g., gap g, period p_1, and diameter D_1. By managing these parameters, the operating frequency can be tuned from f_2 to f_c.

Then, to demonstrate the operating principle of the hybrid metallic vias, Fig. 3(a) shows the equivalent effect of the blind vias and the shorting vias. The blind vias act as the shunt capacitive element C_s between the blind vias and the ground, while the sets of shorting vias serve as the shorting-wall boundary condition. As a result, from Fig. 3(b), we can see that the electric field mainly concentrates under the blind vias instead of the shorting vias. In addition, the capacitive loading blind vias can also compensate for the inductive effect brought from the shorting vias and thus contribute to the good impedance matching of the proposed antenna.

Next, critical parameters of the blind vias are studied to further discuss the working mechanism of the propounded approach. According to the mathematical manipulations in [40], the surface capacitive reactance is mainly affected by gap g, period p_1, and diameter D_1.

Fig. 4 shows the simulated reflection coefficients of the propounded antenna with various parameters g. As seen, minor g brings blind vias a greater surface capacitance, thus reducing the resonance frequency. Adjusting gap g from 2.2 to 1.8 mm results in a reduction in the center resonance frequency from 2.47 to 2.41 GHz. Fig. 5 shows how periods affect the reflection coefficient of the propounded antenna. From 2.1 to 2.5 mm, period p_1 affects the resonance frequency, lowering it from 2.46 to 2.42 GHz. As stationary numbers of blind vias are placed on the two sides, minor period p_1 leads to a shorter loading length, which causes a minor surface capacitance. Fig. 6 shows the simulation results of reflection coefficient of the propounded antenna with respect to various diameters (D_1). The resonance frequency drops from 2.47 to 2.41 GHz when the diameter D_1 varies from 0.9 to 1.3 mm. Due to the greater surface capacitance of blind vias generated by larger D_1, the propounded antenna operates at a lower frequency accordingly. In addition, slightly changing the diameter (D_2) and the period (p_2) of the shorting vias has barely no effect on the operating frequency of the proposed antenna. All these simulated results are consistent with the theory in [40].

III. Antenna Fabrication and Measurement Results

A prototype has been fabricated and tested to validate the design. As shown in Fig. 7(a), a semigrid cable is soldered at the edge of the bottom ground to feed the antenna. The N9917A vector network analyzer is utilized to measure S_{11} of the propounded antenna. As presented in Fig. 7(b), the measured S_{11} achieves good agreement with simulation results. The measurement and simulation S_{11} are both lower than -10 dB from 2.38 to 2.51 GHz. Fig. 8 shows the normalized radiation patterns of the propounded design at 2.44 GHz based on simulation and measurement. It is seen that the simulated result is consistent with the measured result. The proposed structure achieves a broadside radiation pattern with wide beamwidth in both the *yoz* plane and the *xoy* plane. The measured *yoz* plane and *xoy* plane HPBW reach 130° and 160°, respectively. In addition, the cross polarization in the *xoy* plane mainly attributes to the monopole mode. However, this level of cross polarization is acceptable for the access points' application. A permittivity error in fabricated substrates and measurement equipment effects account for the discrepancy between simulation and measurement results.

Fig. 9 shows the total efficiency and realized gain under simulated and measured results, respectively. The simulated realized gain is greater than 3.0 dBi. By utilizing the air cavity with low loss, the simulated total efficiency is greater than 93.7% in the operating band of 2.4–2.48 GHz. According to the measurement results, the

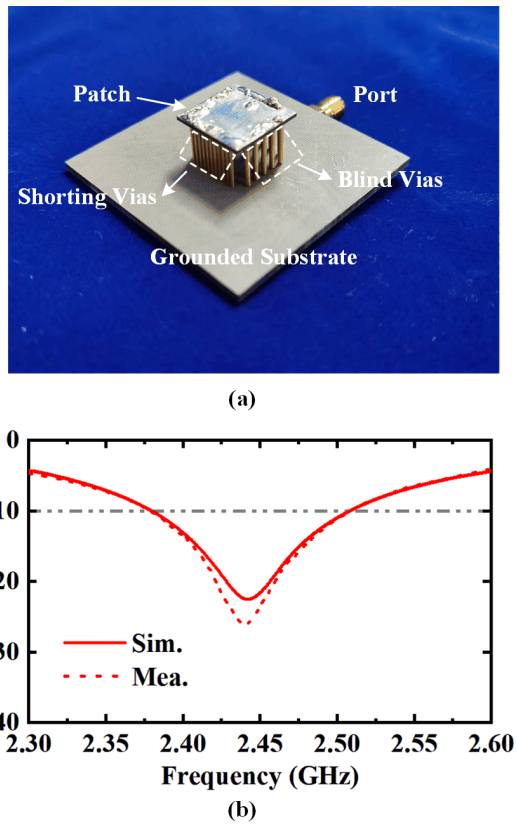

Fig. 7. Antenna measurements. (a) Photograph of fabricated prototype and (b) simulated and measured S_{11}.

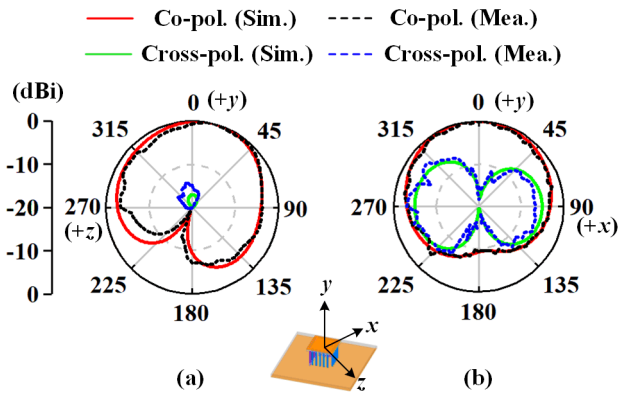

Fig. 8. Normalized simulated and measured radiation patterns of (a) *yoz* plane and (b) *xoy* plane of the proposed antenna at 2.44 GHz.

measured gain is greater than 2.8 dBi and the total efficiency is greater than 90.3% over 2.4–2.48 GHz. The tiny difference between the simulation and measurement data is mostly caused by the fabrication tolerance. To highlight the ascendant and novelty of the propounded antenna, compared with antennas for 2.4 GHz WLAN, we plot a table according to antenna type, size, and efficiency. From Table II, we can see that the approach in [46] occupies a larger dimension to realize the high efficiency. The antenna in [45] has a relatively compact size but fails to achieve high efficiency. It can be concluded that in comparison with the antennas listed in Table II, the propounded antenna is with the competitive ascendency, including the most compact size and the highest radiation efficiency at the same time.

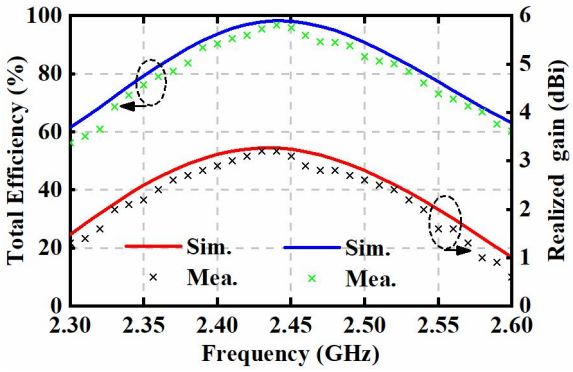

Fig. 9. Simulated and measured gain and total efficiency of the proposed antenna.

TABLE II
COMPARISON AMONG THE PROPOSED DESIGN AND OTHER RELATED ANTENNAS

Reference	Antenna Type	Size(λ_0^3)	Efficiency
[39]	patch	0.19×0.19×0.07	85%
[41]	patch	0.53×0.50×0.01	40%
[42]	patch	0.48×0.48×0.06	34%
[43]	patch	0.45×0.35×0.01	45%
[44]	dipole	0.40×0.36×0.01	50%
[45]	slot	0.24×0.24×0.01	65%
[46]	DRA	0.35×0.20×0.17	86%
Proposed	**patch**	**0.128×0.128×0.1**	**90.3%**

IV. CONCLUSION

In this work, a compact, high-efficiency, and low-cost cage antenna is proposed for WLAN application. By placing hybrid metallized vias, the propounded antenna is miniaturized up to 91.1% compared with the ordinary patch antenna operating at the basic mode. Moreover, by utilizing the air cavity structure, the antenna obtains high total efficiency over 90.3%. To validate the approach, an antenna prototype is fabricated, characterized, and analyzed. The measurement results are with good consistency with the simulation ones, manifesting a total efficiency of 90.3% over the WLAN band (2.4–2.48 GHz). Hence, the propounded approach is with a chance to pave a prospective way for building highly compact and low-latency wireless communication systems.

REFERENCES

[1] C.-H. Wu and T.-G. Ma, "Miniaturized self-oscillating active integrated antenna with quasi-isotropic radiation," *IEEE Trans. Antennas Propag.*, vol. 62, no. 2, pp. 933–936, Feb. 2014.
[2] K.-L. Wong and Y.-C. Chen, "Small-size hybrid loop/open-slot antenna for the LTE smartphone," *IEEE Trans. Antennas Propag.*, vol. 63, no. 12, pp. 5837–5841, Dec. 2015.
[3] Z. Wang, S. Liu, and Y. Dong, "Electrically small, low-Q, wide beam-width, circularly polarized, hybrid magnetic dipole antenna for RFID application," *IEEE Trans. Antennas Propag.*, vol. 69, no. 10, pp. 6284–6293, Oct. 2021.
[4] A. A. Omar, J. Park, W. Kwon, and W. Hong, "A compact wide-band vertically polarized end-fire millimeter-wave antenna utilizing slot, dielectric, and cavity resonators," *IEEE Trans. Antennas Propag.*, vol. 69, no. 9, pp. 5234–5243, Sep. 2021.
[5] R. Xu, Z. Shen, and S. S. Gao, "Compact-size ultra-wideband circularly polarized antenna with stable gain and radiation pattern," *IEEE Trans. Antennas Propag.*, vol. 70, no. 2, pp. 943–952, Feb. 2022.

[6] W. He, Y. He, Y. Li, S.-W. Wong, and L. Zhu, "A compact ultrawideband circularly polarized antenna array with shared partial patches," *IEEE Antennas Wireless Propag. Lett.*, vol. 20, no. 12, pp. 2280–2284, Dec. 2021.

[7] H.-T. Chou and H.-J. Su, "Dual-band hybrid antenna structure with spatial diversity for DTV and WLAN applications," *IEEE Trans. Antennas Propag.*, vol. 65, no. 9, pp. 4850–4853, Sep. 2017.

[8] A. A. Baba, R. M. Hashmi, K. P. Esselle, and A. R. Weily, "Compact high-gain antenna with simple all-dielectric partially reflecting surface," *IEEE Trans. Antennas Propag.*, vol. 66, no. 8, pp. 4343–4348, Aug. 2018.

[9] L. Huitema, M. Koubeissi, M. Mouhamadou, E. Arnaud, C. Decroze, and T. Monediere, "Compact and multiband dielectric resonator antenna with pattern diversity for multistandard mobile handheld devices," *IEEE Trans. Antennas Propag.*, vol. 59, no. 11, pp. 4201–4208, Nov. 2011.

[10] R. Caso, A. D'Alessandro, A. A. Serra, P. Nepa, and G. Manara, "A compact dual-band PIFA for DVB-T and WLAN applications," *IEEE Trans. Antennas Propag.*, vol. 60, no. 4, pp. 2084–2087, Apr. 2012.

[11] S. Das, D. J. Sawyer, N. Diamanti, A. P. Annan, and A. K. Iyer, "A strongly miniaturized and inherently matched folded dipole antenna for narrowband applications," *IEEE Trans. Antennas Propag.*, vol. 68, no. 5, pp. 3377–3386, May 2020.

[12] Y. Hwang, Y. P. Zhang, G. X. Lo, and K. C. Terry, "Planar inverted F antenna loaded with high permittivity material," *Electron. Lett.*, vol. 31, pp. 1710–1712, Sep. 1995.

[13] B. Lee and F. J. Harackiewicz, "Miniature microstrip antenna with a partially filled high-permittivity substrate," *IEEE Trans. Antennas Propag.*, vol. 50, no. 8, pp. 1160–1162, Aug. 2002.

[14] S. Choudhury, A. Mohan, and D. Guha, "Wideband quasi-omnidirectional planar inverted F-antenna for compact wireless systems," *IEEE Antennas Wireless Propag. Lett.*, vol. 17, no. 7, pp. 1305–1308, Jul. 2018.

[15] Y. Saito and T. Fukusako, "Low-profile and electrically small meander-line antenna using a capacitive feed structure," *IEEE Antennas Wireless Propag. Lett.*, vol. 11, pp. 1281–1284, 2012.

[16] Z. Yin, G. He, X.-X. Yang, and S. Gao, "Miniaturized ultrawideband half-mode Vivaldi antenna based on mirror image theory," *IEEE Antennas Wireless Propag. Lett.*, vol. 19, no. 4, pp. 695–699, Apr. 2020.

[17] Y. Gou, S. Yang, Q. Zhu, and Z. Nie, "A compact dual-polarized double E-shaped patch antenna with high isolation," *IEEE Trans. Antennas Propag.*, vol. 61, no. 8, pp. 4349–4353, Aug. 2013.

[18] S. Radavaram and M. Pour, "Wideband radiation reconfigurable microstrip patch antenna loaded with two inverted U-slots," *IEEE Trans. Antennas Propag.*, vol. 67, no. 3, pp. 1501–1508, Mar. 2019.

[19] D. E. Brocker, Z. H. Jiang, M. D. Gregory, and D. H. Werner, "Miniaturized dual-band folded patch antenna with independent band control utilizing an interdigitated slot loading," *IEEE Trans. Antennas Propag.*, vol. 65, no. 1, pp. 380–384, Jan. 2017.

[20] A. Erentok and R. W. Ziolkowski, "Metamaterial-inspired efficient electrically small antennas," *IEEE Trans. Antennas Propag.*, vol. 56, no. 3, pp. 691–707, Mar. 2008.

[21] J. Zhu, M. A. Antoniades, and G. V. Eleftheriades, "A compact tri-band monopole antenna with single-cell metamaterial loading," *IEEE Trans. Antennas Propag.*, vol. 58, no. 4, pp. 1031–1038, Apr. 2010.

[22] S. F. Mahmoud, "A new miniaturized annular ring patch resonator partially loaded by a metamaterial ring with negative permeability and permittivity," *IEEE Antennas Wireless Propag. Lett.*, vol. 3, pp. 19–22, 2004.

[23] A. Alù, F. Bilotti, N. Engheta, and L. Vegni, "Subwavelength, compact, resonant patch antennas loaded with metamaterials," *IEEE Trans. Antennas Propag.*, vol. 55, no. 1, pp. 13–25, Jan. 2007.

[24] C. Pai Yen and A. Alu, "Dual-mode miniaturized elliptical patch antenna with-negative metamaterials," *IEEE Antennas Wireless Propag. Lett.*, vol. 9, pp. 351–354, 2010.

[25] S.-C. Tang, X.-Y. Wang, S. Y. Zheng, Y. M. Pan, and J.-X. Chen, "Frequency-reconfigurable dielectric patch antenna with bandwidth enhancement," *IEEE Trans. Antennas Propag.*, vol. 70, no. 4, pp. 2510–2519, Apr. 2022.

[26] C. Zhou, B. Wang, and H. Wong, "A compact dual-mode circularly polarized antenna with frequency reconfiguration," *IEEE Antennas Wireless Propag. Lett.*, vol. 20, no. 6, pp. 1098–1102, Jun. 2021.

[27] S. Genovesi, A. D. Candia, and A. Monorchio, "Compact and low profile frequency agile antenna for multistandard wireless communication systems," *IEEE Trans. Antennas Propag.*, vol. 62, no. 3, pp. 1019–1026, Mar. 2014.

[28] L. Ge and K.-M. Luk, "A band-reconfigurable antenna based on directed dipole," *IEEE Trans. Antennas Propag.*, vol. 62, no. 1, pp. 64–71, Jan. 2014.

[29] J. Church, J.-C. S. Chieh, L. Xu, J. D. Rockway, and D. Arceo, "UHF electrically small box cage loop antenna with an embedded non-Foster load," *IEEE Antennas Wireless Propag. Lett.*, vol. 13, pp. 1329–1332, 2014.

[30] T. Shi, M.-C. Tang, Z. Wu, H.-X. Xu, and R. W. Ziolkowski, "Improved signal-to-noise ratio, bandwidth-enhanced electrically small antenna augmented with internal non-foster elements," *IEEE Trans. Antennas Propag.*, vol. 67, no. 4, pp. 2763–2768, Apr. 2019.

[31] N. Zhu and R. W. Ziolkowski, "Broad-bandwidth, electrically small antenna augmented with an internal non-Foster element," *IEEE Antennas Wireless Propag. Lett.*, vol. 11, pp. 1116–1120, 2012.

[32] L. J. Chu, "Physical limitations of omni-directional antennas," *J. Appl. Phys.*, vol. 19, no. 12, pp. 1163–1175, Dec. 1948.

[33] R. F. Harrington, "Effect of antenna size on gain, bandwidth, and efficiency," *J. Res. Nat. Bur. Stand*, vol. 64, no. 1, pp. 1–12, Feb. 1960.

[34] J. Ouyang, Y. M. Pan, S. Y. Zheng, and P. F. Hu, "An electrically small planar quasi-isotropic antenna," *IEEE Antennas Wireless Propag. Lett.*, vol. 17, no. 2, pp. 303–306, Feb. 2018.

[35] Z. Wang, Y. Dong, Y. Ning, and T. Itoh, "Miniaturized circularly polarized periodically structured surface antenna for RFID application inspired by SRR," *IEEE Trans. Antennas Propag.*, vol. 69, no. 11, pp. 7269–7277, Nov. 2021.

[36] L. Chang, Z. Zhang, Y. Li, S. Wang, and Z. Feng, "Air-filled long slot leaky-wave antenna based on folded half-mode waveguide using silicon bulk micromachining technology for millimeter-wave band," *IEEE Trans. Antennas Propag.*, vol. 65, no. 7, pp. 3409–3418, Jul. 2017.

[37] P. Liu, Y. Li, Z. Zhang, S. Wang, and Z. Feng, "A fixed-beam leaky-wave cavity-backed slot antenna manufactured by bulk silicon MEMS technology," *IEEE Trans. Antennas Propag.*, vol. 65, no. 9, pp. 4399–4405, Sep. 2017.

[38] J. Hu, Y. Li, S. Wang, and Z. Zhang, "Millimeter-wave air-filled slot antenna with conical beam based on bulk silicon MEMS technology," *IEEE Trans. Antennas Propag.*, vol. 68, no. 5, pp. 4077–4081, May 2020.

[39] Y. He and Y. Li, "Dual-polarized microstrip antennas with capacitive via fence for wide beamwidth and high isolation," *IEEE Trans. Antennas Propag.*, vol. 68, no. 7, pp. 5095–5103, Jul. 2020.

[40] Y. He, Y. Li, L. Zhu, H. Bagci, D. Erricolo, and P.-Y. Chen, "Waveguide dispersion tailoring by using embedded impedance surfaces," *Phys. Rev. A, Gen. Phys.*, vol. 10, no. 6, Dec. 2018, Art. no. 064024.

[41] K.-L. Wong, C.-J. Chen, and W.-Y. Li, "Integrated four low-profile shorted patch dual-band WLAN MIMO antennas for mobile device applications," *IEEE Trans. Antennas Propag.*, vol. 69, no. 6, pp. 3566–3571, Jun. 2021.

[42] R. Caso, A. Michel, M. Rodriguez-Pino, and P. Nepa, "Dual-band UHF-RFID/WLAN circularly polarized antenna for portable RFID readers," *IEEE Trans. Antennas Propag.*, vol. 62, no. 5, pp. 2822–2826, May 2014.

[43] Y. F. Cao, S. W. Cheung, and T. I. Yuk, "A multiband slot antenna for GPS/WiMAX/WLAN systems," *IEEE Trans. Antennas Propag.*, vol. 63, no. 3, pp. 952–958, Mar. 2015.

[44] T. Li, H. Zhai, X. Wang, L. Li, and C. Liang, "Frequency-reconfigurable bow-tie antenna for Bluetooth, WiMAX, and WLAN applications," *IEEE Antennas Wireless Propag. Lett.*, vol. 14, pp. 171–174, 2015.

[45] X. Hu and Q. Zhang, "Compact slot antenna for 2.4 GHz RFID tags," in *Proc. 3rd Eur. Conf. Antennas Propag.*, Jun. 2009, pp. 2796–2798.

[46] L. Guo, K. W. Leung, and N. Yang, "Wide-beamwidth unilateral dielectric resonator antenna using higher-order mode," *IEEE Trans. Antennas Propag.*, vol. 18, no. 1, pp. 93–97, Jan. 2019.